

# Hierarchical copper oxide microspheres prepared in an ordinary household microwave oven

Jiwei Li, Wei Li ✉

Department of Material Science, Taiyuan University of Technology, Taiyuan 030024, People's Republic of China

✉ E-mail: ddwhlw1980@hotmail.com

Published in *Micro & Nano Letters*; Received on 13th December 2018; Revised on 8th February 2019; Accepted on 7th March 2019

Hierarchical copper oxide (CuO) microspheres were prepared by a simple microwave-assisted preparation method in an ordinary household microwave oven under ambient pressure. The CuO microspheres were characterised by scanning electron microscopy, transmission electron microscopy, X-ray diffraction, X-ray photoelectron spectroscopy, and thermal gravimetric analysis. Characterisation results show that the hierarchical CuO microspheres are assembled by spine-like nanorods and have high Brunauer–Emmett–Teller surface area of 25.0 m<sup>2</sup>/g.

**1. Introduction:** Copper oxide (CuO) is one of the most common electrode materials for electrochemical applications such as catalyst, biosensor, and capacitor, due to its chemical stability, non-toxicity, cost-effectiveness, and abundant resources [1–3]. However, the poor electrical conductivity of CuO is a major limitation to achieving high performance of electrochemical device. One effective solution is to optimise the microstructure of CuO to increase the surface contact area between the active materials and the electrolyte, as well as decrease the diffusion paths for charge transfer [4]. In this regard, the hierarchical structure of CuO is particularly attractive to obtain excellent electrochemical performance [5]. Although these reported hierarchical CuO microstructures possess good electrochemical performance, the fabrication methods are usually complex. They often require organic surfactants, special substrates, or structural templates. Therefore, a simple, effective, and environment-friendly method to prepare hierarchical CuO is necessary.

In recent years, green synthesis of nanomaterials is very attractive due to the increasing concern of the environment. Various green nanosynthesis methods such as sonochemical method [6], laser ablation [7], supercritical fluid [8], bio-assistant synthesis [9], and microwave-assisted preparation [10], have been utilised to effectively fabricate nanomaterials with minimum negative consequence on the society and environment. Among these green nanosynthesis methods, microwave-assisted preparation is of great significance [11]. The microwave energy is more environment-friendly, requiring less energy than the conventional heating processes. Besides, compared with the conventional wet chemical method or template method, microwave-assisted preparation has advantages of short processing time, easy operation, and simple control of morphology [10, 11].

In this Letter, we used a simple one-pot microwave-assisted method to fabricate hierarchical CuO microspheres. The growth of this hierarchical CuO microstructure in this work was simply performed in an ordinary household microwave oven while previous CuO nanostructures were fabricated in the custom made microwave ovens which are usually more expensive than domestic microwave ovens. Furthermore, unlike previous CuO nanostructures prepared in a closed vessel with high pressure [12–14], the CuO was prepared under ambient pressure in this work. In these respects, our synthesis process is relatively simple, safe, and low cost [10].

**2. Experimental methods:** All chemicals and solvents, such as copper sulphate pentahydrate (CuSO<sub>4</sub>·5H<sub>2</sub>O), potassium carbonate (K<sub>2</sub>CO<sub>3</sub>), potassium hydroxide (KOH), and hydrochloric acid

(HCl), were obtained from Sinopharm Chemical Reagent Co., Ltd. (Shanghai, China). These reagents possessed the highest commercially pure grade, and they were used without further purification.

A 200 ml aliquot of 0.2 M CuSO<sub>4</sub> solution was quickly poured in 200 ml of 0.8 M K<sub>2</sub>CO<sub>3</sub> solution, and then the mixed solution was immediately placed in an ordinary household microwave oven (Panasonic NN-GF352MXPE). The microwave output was 300 W, and the microwave time was 6 min. The obtained solid product was successively filtered, washed with deionised water and then dried at 50°C for further measurement. For comparison, a typical chemical precipitation method was used to prepare CuO. A 40 ml aliquot of 4 M K<sub>2</sub>CO<sub>3</sub> solution was added dropwise into 400 ml of 0.1 M CuSO<sub>4</sub> solution under mechanical stirring. The precipitate was filtered, washed, dried, and finally annealed at 250°C for 3 h. For convenience, the sample prepared by the microwave-assisted method was named W–CuO, and the sample prepared by the conventional chemical precipitation method was denoted as H–CuO.

Scanning electron microscopy (SEM) measurements were carried out with a JSM-7500 instrument (JEOL, Japan). Transmission electron microscopy (TEM) was carried out with a Tecnai-G20 instrument (FEI, USA). X-ray photoelectron spectroscopy (XPS) was performed with an Amicus Budget spectrometer (Shimadzu, Japan) using Mg K $\alpha$  X-ray source (1253.6 eV) operating at 10 kV and 10 mA. X-ray diffraction (XRD) was performed with a TD3500 X-ray diffractometer (TONGDA, China) with Cu K $\alpha$  radiation ( $\lambda = 1.5418 \text{ \AA}$ ). Thermal gravimetric analysis was performed with a thermal analysis equipment (STA 449F3, NETZSCH, Germany). The experiments were carried out at a heating rate of 10 K min<sup>-1</sup> over a temperature ranging from room temperature to 500°C with an N<sub>2</sub> flow rate of 50 ml min<sup>-1</sup>. The Brunauer–Emmett–Teller (BET) measurement was conducted at 77 K under N<sub>2</sub> with an ASAP2000 instrument (Micromeritics, USA).

**3. Results and discussion:** Typical SEM images are shown in Fig. 1. Unlike the irregular granular structure of H–CuO (Fig. 1a), W–CuO exhibits a more regular spherical morphology with a diameter ranging from 300 nm to 1  $\mu$ m (Fig. 1b). Fig. 1a also shows a few big clusters which are expectable for a typical chemical precipitation method because some nanoparticles formed in the early stage may act as growth cores and then, be surrounded by metal oxides formed in the later stage [15]. In addition, the high-magnification SEM picture reveals hierarchical waxberry-like microspheres (inset of Fig. 1b).

The TEM picture, which was used to investigate the detailed microstructure, further confirms the hierarchical waxberry-like spherical morphology of W-CuO (Fig. 2b). The hierarchical W-CuO microspheres are assembled with spine-like nanorods (Fig. 2d). High-resolution TEM (HRTEM) images show that randomly oriented H-CuO nanocrystals are  $\sim 7\text{--}10$  nm in size (Fig. 2e). Unlike the granular structure of H-CuO, W-CuO exhibits a lamellar structure usually observed in some 2D materials, such as graphene or MoS<sub>2</sub> (Fig. 2f). The lattice distance in HRTEM images is  $\sim 0.25$  nm, which corresponds to the (002) plane of the CuO crystal phase.

The XRD patterns of CuO are shown in Fig. 3. The diffraction peaks can be assigned to a monoclinic structure of CuO (JCPDS Card No. 80-1916). No characteristic peaks of possible impurities, such as Cu(OH)<sub>2</sub> or Cu<sub>2</sub>O, appear, indicating the phase purities of W-CuO and H-CuO.

The complete XPS spectra from 0 to 1000 eV are shown in Fig. 4a. The increase in XPS background can be attributed to the scattering of photoelectrons from Cu ions during photoelectron transfer to the CuO surface [16]. The Cu 2p spectra are used to determine the oxidation state of Cu. The main Cu 2p<sub>3/2</sub> and Cu 2p<sub>1/2</sub> peaks, together with their shake-up satellite peaks are

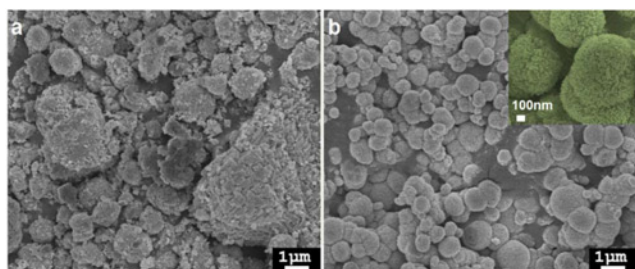


**Fig. 1** SEM images of  
a H-CuO and  
b W-CuO. Inset of (b) is the high-magnification picture of W-CuO microspheres

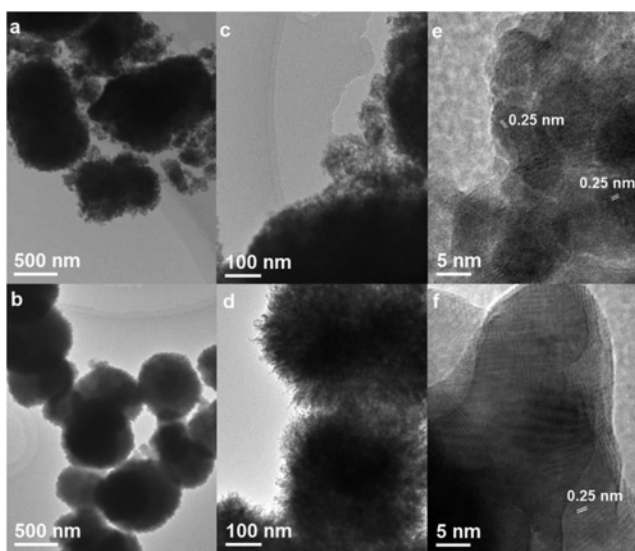


**Fig. 2** TEM images of  
a H-CuO 500 nm  
b W-CuO 500 nm  
c H-CuO 100 nm  
d W-CuO 100 nm  
e High-resolution TEM images of H-CuO 5 nm  
f W-CuO 5 nm

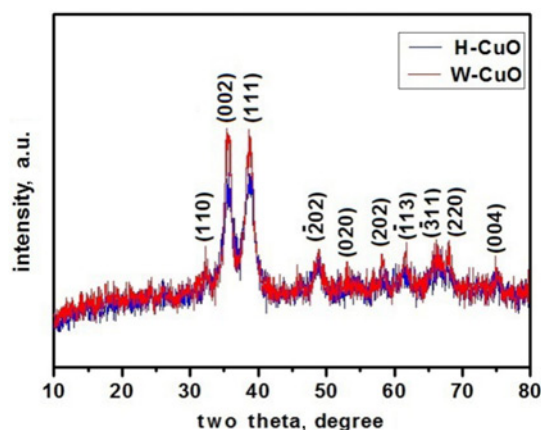


**Fig. 3** XRD patterns of H-CuO and W-CuO

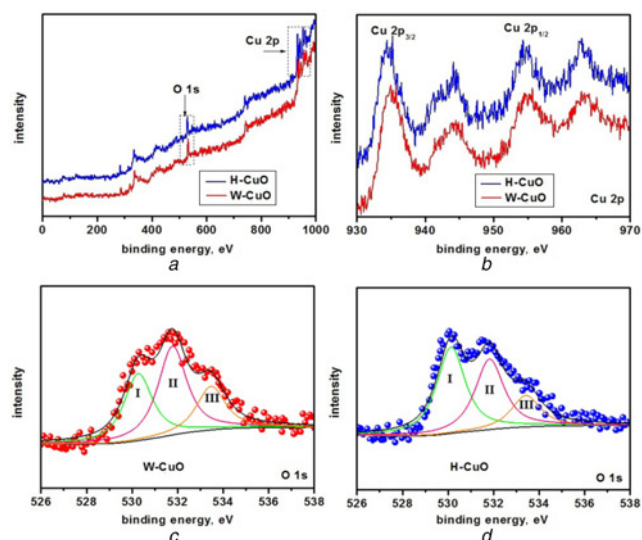


**Fig. 4** Complete XPS spectra of samples  
a Complete XPS spectra of samples  
b Core-level XPS spectra of Cu 2p state  
c Core-level XPS spectrum of O 1s state of W-CuO  
d Core-level XPS spectrum of O 1s state of H-CuO

clearly evidenced. CuO and Cu<sub>2</sub>O are two semiconducting phases of CuO. The existence of satellite peaks indicates the formation of CuO [17]. However, the Cu 2p<sub>3/2</sub> peak, which may be integrated from any combination of Cu<sub>2</sub>O, Cu, or CuO peak, is difficult to interpret because Cu and Cu<sub>2</sub>O have nearly similar binding energies. In this situation, the LMM-2 auger transition peak in XPS spectra, namely, 568 eV for Cu and 570 eV for Cu<sub>2</sub>O, is generally used as a strong evidence for their presence [16]. We find that no peak appears in this region, indicating the sole existence of CuO. Therefore, according to the XPS study of Cu 2p, the oxidation state of Cu is +2, and CuO is confirmed as the final product.

The O 1s spectra are used to determine the surface composition of CuO. The O 1s peak can be decomposed into three meaningful component peaks, which are marked as I, II, and III. Peak I can be assigned to oxygen from lattice oxide. Peaks II and III originated from surface chemical compounds that contain oxygen atoms. In specific, peak II is related to the oxygen atoms in hydroxyl and carbonate groups, whereas peak III corresponds to the surface-adsorbed water [18, 19]. Comparison of the integrated area of peak I with the sum of the integrated areas reveals that the percent of oxygen from the lattice oxide is 33.6 and 45.8% for W-CuO and H-CuO, respectively, indicating that W-CuO has

more surface compounds, such as hydroxyl group and adsorbed water than H-CuO [20].

The two wide peaks in the derivative thermogravimetry (DTG) curve clearly indicate two stages during the heating process from ambient temperature to 500°C (Fig. 5). The first stage is related to the evaporation of surface-adsorbed water, and the second stage is the loss of hydroxyl and carbonate groups [21]. The TGA curves show that the final remaining weight percentages of W-CuO and H-CuO are ~87.13 and 95.57%, respectively. The possible reason is related to the hierarchical spherical microstructure through which W-CuO possesses higher surface area and, therefore, has more adsorption sites than H-CuO [21, 22]. The TGA-DTG curve nearly plateaus at over 350°C, indicating that both W-CuO and H-CuO undergo insignificant weight loss in this temperature range.

Nitrogen adsorption/desorption method was used to further investigate the surface area and porous feature of W-CuO. The isotherm profile is shown in Fig. 6. The isotherm is a typical IV type curve, indicating a porous structure of W-CuO. The calculated BET surface area of W-CuO (25.0 m<sup>2</sup>/g) is much higher than that of H-CuO (18.0 m<sup>2</sup>/g) and commercial CuO (0.1 m<sup>2</sup>/g) [23].

Electrochemical impedance spectroscopy was carried out to investigate the charge transport properties of the microspheres. The Nyquist plot, which shows a semicircle in the high-frequency region and a line in the low-frequency region, is shown in Fig. 7. The semicircle can be attributed to a kinetic (charge transfer) controlled process on the electrode-electrolyte interface while the line indicates a mass transfer controlled process on the electrode-electrolyte interface [24, 25]. Both plots have a steep line in the low-frequency region, indicating that the diffusion of the electrolyte is quite fast within these two oxides. Nevertheless, W-CuO possesses

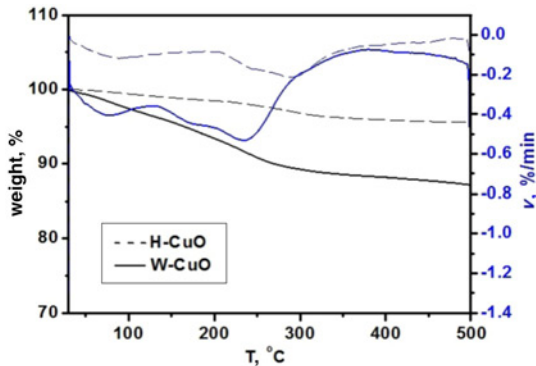


Fig. 5 TG-DTG curves of H-CuO and W-CuO

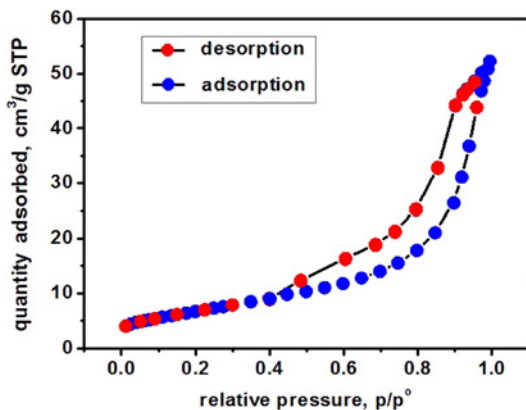


Fig. 6 N<sub>2</sub> adsorption-desorption isothermal curve of W-CuO

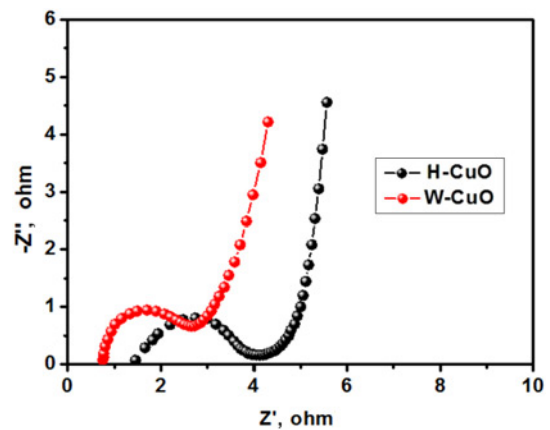


Fig. 7 Nyquist impedance plots for H-CuO and W-CuO electrodes

a smaller semicircle than H-CuO, suggesting that W-CuO has a lower charge transfer resistance than H-CuO. The small charge transfer resistance of W-CuO is related to the lamellar microstructures, which can guarantee a larger electroactive surface area for remarkable charge diffusion [26].

**4. Conclusion:** The hierarchical CuO microspheres (W-CuO) can be prepared by a simple, safe, fast, and low-cost microwave-assisted method in an ordinary household microwave oven under ambient pressure. The W-CuO exhibits a relatively narrow size distribution in the comparison with H-CuO prepared by conventional chemical precipitation method. Due to the lamella-like nanorod blocks of microspheres, the W-CuO has a higher surface area and hence, exhibit better charge transport performance as electrode material than H-CuO. Future works may focus on the application of W-CuO as well as the synthesis of other type of metal oxides.

**5. Acknowledgments:** This work was supported by the National Natural Science Foundation of China (grant no. 61501318).

## 6 References

- [1] Zhao B., Liu P., Zhuang H., *ET AL.*: 'Hierarchical self-assembly of microscale leaf-like CuO on graphene sheets for high-performance electrochemical capacitors', *J. Mater. Chem. A*, 2013, **1**, pp. 367-373
- [2] Chen W., Li R.Y., Li Z.J., *ET AL.*: 'Promising copper oxide-histidine functionalized graphene quantum dots hybrid for electrochemical detection of hydroquinone', *J. Alloy. Compd.*, 2018, **777**, pp. 1001-1009
- [3] Malkani A.S., Dunwell M., Xuo B.J.: 'Operando spectroscopic investigations of copper and oxide derived copper catalysts for electrochemical CO reduction', *ACS Catal.*, 2019, **9**, pp. 474-478
- [4] Kate R.S., Khalate S.A., Deokate R.J.: 'Overview of nanostructured metal oxides and pure nickel oxide (NiO) electrodes for supercapacitors: a review', *J. Alloy. Compd.*, 2018, **734**, pp. 89-111
- [5] Ye J., Li Z., Dai Z., *ET AL.*: 'Facile synthesis of hierarchical CuO nanoflower for supercapacitor electrodes', *J. Electron. Mater.*, 2016, **45**, pp. 4237-4245
- [6] Neto N.F.A., Oliveira P.M., Nascimento R.M., *ET AL.*: 'Influence of pH on the morphology and photocatalytic activity of CuO obtained by sonochemical method using different surfactants', *Ceram. Int.*, 2018, **45**, pp. 651-658
- [7] Gavrilenco E.A., Goncharova D.A., Lapin I.N., *ET AL.*: 'Comparative study of physicochemical and antibacterial properties of ZnO nanoparticles prepared by laser ablation of Zn target in water and air', *Materials*, 2019, **12**, p. 186
- [8] Byrappa K., Ohara S., Adschiri T.: 'Nanoparticles synthesis using supercritical fluid technology-towards biomedical applications', *Adv. Drug Deliv. Rev.*, 2008, **60**, pp. 299-327
- [9] Focsan M., Gabudean A.M., Canpean V., *ET AL.*: 'Formation of size and shape tunable gold nanoparticles in solution by bio-assisted synthesis with bovine serum albumin in native and denatured state', *Mater. Chem. Phys.*, 2011, **129**, pp. 939-942

- [10] Zhu Y., Chen F.: 'Microwave-assisted preparation of inorganic nanostructures in liquid phase', *Chem. Rev.*, 2014, **114**, pp. 6462–6555
- [11] Schütz M.B., Xiao L., Lehnen T., *ET AL.*: 'Microwave-assisted synthesis of nanocrystalline binary and ternary metal oxides', *Int. Mater. Rev.*, 2018, **63**, pp. 341–374
- [12] Poienar M., Banica R., Sfirloaga P., *ET AL.*: 'Microwave-assisted hydrothermal synthesis and catalytic activity study of crednerite-type  $\text{CuMnO}_2$  materials', *Ceram. Int.*, 2018, **44**, pp. 6157–6161
- [13] Volanti D.P., Orlandi M.O., Andres J., *ET AL.*: 'Efficient microwave-assisted hydrothermal synthesis of  $\text{CuO}$  sea urchin-like architectures via a mesoscale self-assembly', *CrystEngComm*, 2010, **12**, pp. 1696–1699
- [14] Mishra A.K., Nayak A.K., Das A.K., *ET AL.*: 'Microwave-assisted solvothermal synthesis of cupric oxide nanostructures for high-performance supercapacitor', *J. Phys. Chem. C*, 2018, **122**, pp. 11249–11261
- [15] Wang N., Cai Y., Zhang R.Q.: 'Growth of nanowires', *Mater. Sci. Eng. R*, 2008, **60**, pp. 1–51
- [16] Ghodselahi T., Vesaghi M.A., Shafiekhani A., *ET AL.*: 'XPS study of the  $\text{Cu@Cu}_2\text{O}$  core-shell nanoparticles', *Appl. Surf. Sci.*, 2008, **255**, pp. 2730–2734
- [17] Guan P., Li Y., Zhang J., *ET AL.*: 'Non-enzymatic glucose biosensor based on  $\text{CuO}$ -decorated  $\text{CeO}_2$  nanoparticles', *Nanomaterials*, 2016, **6**, p. 159
- [18] Şişman O., Kılınc N., Öztürk Z.Z.: 'Structural, electrical and  $\text{H}_2$  sensing properties of copper oxide nanowires on glass substrate by anodization', *Sens. Actuator B*, 2016, **236**, pp. 1118–1125
- [19] Bialas A., Kondratowicz T., Drozdek M., *ET AL.*: 'Catalytic combustion of toluene over copper oxide deposited on two types of yttria-stabilized zirconia', *Catal. Today*, 2015, **257**, pp. 144–149
- [20] Lee S.H., Stewart R.J., Park H., *ET AL.*: 'Effect of nanoscale roughness on adhesion between glassy silica and polyimides: a molecular dynamics study', *J. Phys. Chem. C*, 2017, **121**, pp. 24648–24656
- [21] Wang Y., Zhang C., Bi S., *ET AL.*: 'Preparation of  $\text{ZnO}$  nanoparticles using the direct precipitation method in a membrane dispersion micro-structured reactor', *Powder Technol.*, 2010, **202**, pp. 130–136
- [22] Tian B., Qiao Y., Tian Y., *ET AL.*: 'Investigation on the effect of particle size and heating rate on pyrolysis characteristics of a bituminous coal by TG-FTIR', *J. Anal. Appl. Pyrol.*, 2016, **121**, pp. 376–386
- [23] Wang J., Liu Y., Wang S., *ET AL.*: 'Facile fabrication of pompon-like hierarchical  $\text{CuO}$  hollow microspheres for high-performance lithium-ion batteries', *J. Mater. Chem. A*, 2014, **2**, pp. 1224–1229
- [24] Li Y., Chang S., Liu X., *ET AL.*: 'Nanostructured  $\text{CuO}$  directly grown on copper foam and their supercapacitance performance', *Electrochim. Acta*, 2012, **85**, pp. 393–398
- [25] Xu W., Dai S., Liu G., *ET AL.*: ' $\text{CuO}$  nanoflowers growing on carbon fiber fabric for flexible high-performance supercapacitors', *Electrochim. Acta*, 2016, **203**, pp. 1–8
- [26] Moosavifard S.E., El-Kady M.F., Rahmanifar M.S., *ET AL.*: 'Designing 3D highly ordered nanoporous  $\text{CuO}$  electrodes for high performance asymmetric supercapacitors', *ACS Appl. Mater. Int.*, 2015, **7**, pp. 4851–4860